In silico analysis shows that dynamic changes in curvature guide cell migration over long distances

Ian Manifacier (1)(2), Gildas Carlin (1)(2), Dongshu Liu (1)(2), Maxime Vassaux (3), Laurent Pieuchot (4), Valeriy Luchnikov (4), Karine Anselme (4), Jean-Louis Milan* (1)(2)

1. *Aix Marseille University, CNRS, ISM, Marseille, France*
2. *APHM, Institute for Locomotion, Department of Orthopaedics and Traumatology, St Marguerite Hospital, Marseille, France*
3. *IPR Institute of Physics, UMR UR1 CNRS 6251, Rennes 1 University, France*
4. *Université de Haute-Alsace, CNRS, IS2M, UMR 7361, Mulhouse F-68100, France.*

**corresponding author*

Abstract

In-vitro experiments have shown that cell scale curvatures influence cell migration; cells avoid convex hills and settle in concave valleys. However, it is not known whether dynamic changes in curvature can guide cell migration. This study extends a previous in-silico model to explore the effects over time of changing the substrate curvature on cell migration guidance. By simulating a dynamic surface curvature using traveling wave patterns, we investigate the influence of wave height and speed, and find that long-distance cell migration guidance can be achieved on specific wave patterns. We propose a mechanistic explanation of what we call *dynamic curvotaxis* and highlight those cellular features that may be involved. Our results open a new area of study for understanding cell mobility in dynamic environments, from single-cell in-vitro experiments to multi-cellular in-vivo mechanisms.

Keywords

Curvature, cell migration, curvotaxis, long-distance cell migration, modeling, contractility, nucleus

1. Introduction

Multiple environmental factors guide cell migration and some of the best-known factors include soluble and extracellular matrix bound chemical gradients respectively referred to as chemotaxis [Devreotes2003] and haptotaxis [Chelberg1989]. More recent findings showed that cell migration is also directed by purely mechanical cues, such as stiffness gradients (durotaxis) [Lo2000; Isenberg2009], topographic pattern gradients (topotaxis) [Park2018], and topography anisotropy (ratchetaxis) [Jiang2005; Caballero2015a, Caballero2015b]. In this last case, called ratchetaxis, cells simply choose the direction that minimizes cellular deformation and energy expenditure. In addition, Reversat et al. 2020 showed that confined leukocytes are guided by topographic features as they migrate using retrograde actin flow, without adhering or pulling on the substrate [Reversat2020].

Mounting experimental evidence based on static substrates indicates that curvature influences single and multi-cellular migration [Malheiro2016; Pieuchot2018; Vassaux2019; Callens2020]. For example, mesenchymal stem cells and fibroblast cells cultured on a surface landscape that was defined by rolling

hills and valleys were shown to be significantly affected by cell-scale curvature [Pieuchot2018]. Interestingly, cells would avoid going over convex hills by clearly steering around them and were more likely to go settle in concave valleys. No nuclei were positioned on the area representing the 20% most convex parts of the substrate, while over 60% of nuclei were positioned in the most concave valleys of equal size. Flipping the substrate over showed that gravity was not involved. Consequently, the influence of substrate curvature on cell migration is called curvotaxis [Pieuchot2018]. Curvotaxis requires a dynamic interplay between the nucleus and the cytoskeleton, and more precisely we know that nuclear integrity and actomyosin contractility are needed for curvotaxis. Disrupting either prevents curvotaxis from occurring [Pieuchot2018]. The actin cytoskeleton and the nucleus have direct mechanosensitive links between each other that regulate a range of cellular processes including nuclear positioning, while nuclear positioning influences cell polarization prior to migration [Luxton2011; Davidson2021]. This mechanosensitive linkage is in part explained by the small Rho GTPases Cdc42 which is involved in the regulation of the actin cytoskeleton, and the myotonic dystrophy kinase-related Cdc42-binding kinase (MRCK) pathway which promotes nuclear movement by forming transmembrane actin-associated nuclear (TAN) lines composed of transverse actin cables linked to Nesprin-2 [Luxton2010; Davidson2021]. Moreover, the centrosome which is associated with the nucleus membrane plays also a role in the initiation of cell polarization and directional cell migration [Zhang2017]. Interestingly, as cells traversed a curved landscape, the nucleus was generally offset closer to concave valleys than the barycenter of the cell [Pieuchot2018]. These findings lead us to create a computer model in Vassaux et al. 2019 to physically explain the mechanobiological process of curvotaxis based on key known parameters, such as cell contractility and nucleus positioning [Vassaux2019]. In-silico analysis showed that the nucleus acts as a mechanical sensor that leads the migrating cell toward concave areas. Curvature-induced motion of the nucleus towards concave areas can be explained by the difference in mechanical constraints applied on the nucleus by the cytoskeleton between convex and concave areas. Simulation results from Vassaux et al. 2019 showed that dragging the nucleus toward convex surfaces required more mechanical energy, while adhesion repositioning towards concave regions was energetically more efficient [Vassaux2019]. From a physical perspective, it consequently becomes harder for the cell to drag its nucleus toward convexities than to nudge it to concavities. However, hill and valley substrates cannot direct cell migration in a given direction, nor over long distances. Instead, such substrates can only bias cell migration which favors concave regions.

Interestingly, another single cell study on cylinder shaped substrates showed that stromal cells adjusted their speed and directional persistence in function of substrate curvature [Werner2019]. On the inner surface of the cylinder, cell migration was isotropic; this implies that movement of the cells is not affected by concavity. On the contrary, cells cultivated on the convex outer surface of cylinders were aligned and migrated primarily parallel to the axis of the cylinder and were able to move both ways along this axis.

The examples above clearly demonstrate that curvature influences migration by restricting cell motion, but none clearly show that reliable cell guidance over long distances can be achieved in a given direction. Long distance migration is often observed in-vivo during development. Indeed, in embryonic development, various types of processes rely on directed cell migration over long distances [Kishi2014; Scarpa2016; SenGupta2021]. Long-distance directed cell migration is essential for proper organ morphogenesis [Theveneau2012; Scarpa2016; Shellard2020] as well as the formation of new blood vessels [Patan2004; Otrock2007; Arima2011]. Furthermore, embryonic development involves various events where tissues contract [Shellard2018; Bailles2019], bend and shift [Harmand2021]. This means that cells are exposed to dynamic topography, including curvature changes and even curvature inversion as the surrounding tissues

grow and develop [Schamberger2023]. In addition, various examples of calcium-mediated contraction waves are known to influence morphogenesis during the early stages of development [Chevalier2018; Bailles2019]. For instance, in drosophila, reversible millihertz contractions of the surrounding tissue were shown to induce cell ingression [Sokolow2012]. Moreover, the early embryo is composed of several cell layers and during development there are numerous examples of folds, furrows, and invaginations that induce dynamic changes in curvature. For instance, many slow calcium waves are seen as indentation waves [Jaffe1998; Jaffe2008]. As one layer transiently contracts due to calcium wave propagation, cells in adjacent layers may perceive these contractions as dynamic topographic variations, similar to traveling waves that move up and down [Jaffe1998; Jaffe2008]. This raises the question of how cells can be influenced by dynamic curvature. On another note, some cell types are more prone to curvotaxis than others [Pieuchot2018] suggesting that in vivo and/or in vitro cell sorting by dynamic curvature is plausible.

The examples above allow us to consider a mechanism by which curvature can dynamically change to stimulate and direct cell migration. We hypothesize that cell migration guidance can be achieved over long distances by continuously exposing cells to a curvature gradient. We know that on landscapes composed of hills and valleys, cells preferentially migrate towards valleys. We can therefore deform the landscape continuously so that valleys are always ahead of the cell and hills behind and one solution would be the production of traveling waves at the surface of the substrate. Over the past 20 years, significant developments have been made in cellular substrate engineering to study and control cell migration [Hersen2011; Le Digabel2011; Han2012; Pieuchot2018; Ribeiro2016]. Although there is a plethora of substrates that were engineered to influence cell migration [Dokukina2010; Caballero2015b, Caballero2015a] and some are dynamic [Raghavan2010], only a few change their shape dynamically [le Digabel2011; Chandorkar2019]. Some can change their topology on the submicrometric scale [Chandorkar2019] but none currently fit the requirements to test our hypothesis. Setting up an experiment to test our hypothesis would still require significant technical development. While it is not yet possible to produce cell-scale traveling waves, some of us have developed deformable substrates capable of switching from a flat to a wavy state. These substrates have been used to monitor the behavior of cells during switching and deformation of the substrate and consequently, during the local change of the substrate curvature as well. These studies show that the cells are able to dynamically detect a change in curvature. Substrate undulation induced cell migration over very short distances, away from convex peaks and until concave valleys are reached [Tomba2019].

At the cost of some biological simplifications, in-silico modeling may provide valuable insight into cell behavior and inner mechanisms despite current experimental limitations. Previous studies simulated cell migration on curved substrates using phase-field models [Löber2014; Tjhung2015]. These models describe cell migration as a lamellipodium-based motion within a continuous medium that represents the cell and its contractile cytoskeleton, solving cell migration as a moving boundary problem where the boundary is the cell membrane. The cell interior is represented by an active gel that is able to polymerize or depolymerize and contract, which generates actin flow. For instance, the phase-field models revealed that confinement, substrate curvature, and topography modulate the cell's speed, shape, and actin organization and can induce changes in the direction of motion along axes defined by the constraints [Marzban2019; Winkler2019]. Nonetheless, these models do not describe the real architecture of the cytoskeleton, nor do they consider the interplay between the nucleus and the cytoskeleton, yet these are known to be involved during curvotaxis. Our divided medium cell model does accomplish this, even though representations of lamellipodium and focal adhesions are rudimentary.

The effect of dynamic substrate curvature on cell migration has not been studied, not even in-silico. We hypothesize that dynamic curvature can guide cell migration. Here we propose testing the hypothesis using an in-silico model developed by Vassaux et al. 2019 on our computational cell model. This cell model was previously validated as able to reproduce curvotaxis on static curvatures. We extrapolated the domain of application of the cell model to the case of dynamic curvature by submitting it to slowly travelling waves. As a result, in each simulation, the cell model can predict a migration trajectory on a slowly moving substrate with negligible inertia effects. We can therefore reasonably assume that this application of the cell model to dynamic curvotaxis, is safe and consistent. Simulation results show that single cells are able to undergo dynamic curvotaxis over long distances when subject to traveling waves. Increasing wave height increases the speed at which cells are able to follow the traveling waves. We propose a mechanistic explanation of dynamic curvotaxis by highlighting the cellular features that are likely involved. Simulations indicate that cell migration speed depends on wave slope together with intrinsic mechanical properties of the cells such as contractility, spread area and focal adhesion distribution. This relationship is necessary to match the wave pattern speed with cell speed and to generate continuous guidance in cell migration. Finally, to offer a first virtual proof-of-concept for dynamic curvotaxis, we defined substrate specifications to reliably achieve sustained migration.

2. Method

The cell structure and cytoskeleton are modeled as a system of multiple mechanical interactions. The cell is subdivided into numerous rigid spherical particles that interact mechanically with each other via contact, cable, and spring interactions. These interactions represent the mechanical forces produced or supported by the various filament networks that compose the cytoskeleton and nucleoskeleton. The cell model used in this study was previously developed and validated to provide an explanation for curvotaxis on static substrates [Vassaux2019]. Here, the extrapolated model is well adapted to test whether, in conjunction with curvotaxis, traveling waves can lead to sustained long-distance cell migration. The cell model adheres on a dynamic substrate which is a moving surface that is also subdivided into rigid spheres.

2.1 Mechanical modeling paradigms

Laws of motion

The rigid spheres composing the cell model and the substrate can mechanically interact with one another through predefined contact and cohesive forces and these spheres are ultimately subject to a numerical adaptation of Newton's laws of motion:

$$\underline{F_i} + \sum_{j=1}^{N} \underline{F_{i,j}} = m_i \underline{a_i}$$

where respectively $\underline{F_i}$, m_i and $\underline{a_i}$, represent the external force vector (boundary condition) applied to the particle i, its mass, and acceleration vector. Notation-wise, vectors are distinguished from scalars by underlining the variable. $\underline{F_{i,j}}$ is the force of the interaction between the particles i and j, while N is the number of other particles from the cell model or the substrate which interact with particle i.

Compressive contacts

Particles repel each other via frictionless contact interactions defined by the Signorini's contact problem, and are resolved numerically via the *Non-Smooth Contact Dynamics* (NSCD) implicit solution algorithm [Jean1999]. Here is how this Frictionless contact is defined:

$$F_{i,j}^{ct} \geq 0\ ;$$

$$g_{i,j} - \left(r_i + r_j\right) \geq 0;$$

$$F_{i,j}^{ct}.\left(g_{i,j} - \left(r_i + r_j\right)\right) = 0$$

where $F_{i,j}^{ct}$ is the magnitude of the force of contact applied by the particle j on i; $g_{i,j} = \left|\underline{x}_i - \underline{x}_j\right|_2$ is the gap between centroids of the particles i and j, with $\underline{x}$ the position vector; r_i and r_j are radii of the particles i and j.

Spring interactions

A spring interaction enables two particles to push and pull one another.

$$F_{i,j}^{sp} = k_{i,j}\left(\frac{g_{i,j} - g_{i,j}^0}{g_{i,j}^0} + \tau_{i,j}\right)$$

where $F_{i,j}^{sp}$ is the magnitude of the spring force applied by the particle j on particle i, $k_{i,j}$, $g_{i,j}$, $g_{i,j}^0$ and $\tau_{i,j}$ respectively represent the stiffness defined as force per strain, the current length, the initial length, and the pre-strain of the cable linking the particles i and j.

Cable interaction

Unlike a spring interaction, a cable interaction only allows a particle pair to pull on each other, it therefore cannot bear compression loads. Particles only pull on each other when the distance between the two particles exceeds the rest length of the cable.

$$F_{i,j}^{ca} = \left\langle k_{i,j}\left(\frac{g_{i,j} - g_{i,j}^0}{g_{i,j}^0} + \tau_{i,j}\right)\right\rangle_+$$

Above, $F_{i,j}^{ca}$ is the magnitude of the cable traction force applied by the particle j on the particle i. The stiffness $k_{i,j}$ is defined as force per strain, which in turn corresponds to the product of the cross section with Young's modulus. $g_{i,j}$, $g_{i,j}^0$ and $\tau_{i,j}$ respectively represent: the current length, the initial length, and the pre-strain of the cable linking the particles i and j. The brackets $\langle . \rangle +$ refer to the positive part of the scalar in between, while any non-positive value will be considered null. Considering a positive pre-strain means that the interaction is initially under tension. Inversely, a negative pre-strain means that there is some initial slack in the interaction.

2.2 Cell model structure

Initially the cell had a spherical shape 20 μm in diameter and was composed of various concentric layers of spherical bodies. The cytoskeleton (CSK) is generated probabilistically with a low degree of randomness (intermediate filaments, microfilaments, microtubules and stress fibers) in order to introduce some slight anisotropy in the cell structure. The outer layer of spherical contact points represents the cell membrane and actin cortex. This outer layer was made of overlapping particles to prevent the particle contained within from escaping. The next inward layer represented the cytosol, modeled as dense spherical particle packing, and in the middle was the nucleus. Initially, the latter was 10 μm in diameter and was composed of a nuclear envelope and the nucleoskeleton.

The cell membrane and the cytosol amounted to about 2850 particles, while the nucleus and nuclear membrane total approximately 2300 particles, totaling approximately 5150 particles (depending on the outcome of the pre-processing algorithm). These spherical particles were mechanically connected via the interactions detailed below and were assigned the density of water.

The inner nucleus

The inner part of the nucleus (IN) is considered to be an incompressible fluid, represented by a dense poly-disperse packing of spherical particles with a radius between 0.4-0.65 μm. Inner nucleus particles only interact with each other by compressive contact.

Nuclear membrane

The nuclear membrane (NM) is defined by a single layer of overlapping particles, with a radius of 0.33μm encapsulating all inner nuclear particles. With the initial overlap of particles, the nucleus membrane could be considered as an impermeable envelope that prevents inner nuclear particles from escaping.

Nuclear membrane particles are connected to each other via cable interactions of stiffness k_{NM} and a positive pre-strain τ_{CM}. Nuclear membrane particles interact by contact between inner nuclear and cytosolic particles. Nuclear membrane particles also initially overlap with one another enough to allow the nuclear membrane to stretch, yet remain impermeable.

Cytosol

Similar to the inner nucleus, the cytosol (CTS) is considered an incompressible fluid and is thus modeled as a dense poly-disperse packing of spherical particles with a radius between 0.1-2.0μm. Cytosolic particles can interact by contact with each other, with nuclear membrane, and with the cell membrane particles.

Cell membrane

This cell membrane (CM) is initially defined by a single layer of overlapping particles, with a radius 1.0µm, that encapsulates all inner cell particles. As with the nucleus membrane, with the initial overlap of particles, the cell membrane could be considered as an impermeable envelope that prevents inner cellular particles from escaping. Membrane particles are connected to each other by cable interactions of stiffness k_{CM} and pre-strain τ_{CM}.

However, the cell and nucleus membranes are not totally impermeable in the model. On rare occasions, when the membrane stretches too much, a few inner particles may escape. If only a few out of thousands escape, we consider the membrane to be sufficiently impermeable. The impermeability of cell and nuclear membranes was therefore verified empirically.

Focal adhesions

The cell model adheres on the substrate via 30 focal adhesions (FA) initially located on the basal side. Each focal adhesion is composed of a single particle that is connected to neighboring cell membrane particles initially closer than l_{FA}. The connection between the focal adhesion particles and the cell membrane counterpart is achieved via tension cables of positive pre-strain τ_A, and of stiffness k_{FA}.

Actin microfilaments

The actin microfilament (MF) network is modeled by positively pre-strained [Milan2016] τ_{MF} cable interactions connecting preselected particles within the cytosol where the initial distance each from the other is lower than l_{MF}.

Stress fibers

Stress fibers (SF) are linear structures created by interconnecting particles throughout the cytosol with positively pre-strained τ_{SF} tension cables of stiffness k_{SF}. Each stress fiber initiates at a focal adhesion and either terminates at another focal adhesion or at the dorsal part of the cell membrane.

Microtubules

Unlike the two previous networks of filaments, microtubules (MT) are able to sustain compression, therefore they are considered instead as a network of interconnected springs. A particle of the set is assumed to interact with other particles of the set located at an initial distance lower than l_{MT}. The MT are generated from the centrosome, namely a specific location of the CSK linked to the nucleus.

Intermediate filaments

Intermediate filaments (IF) are modeled as slack cables interconnecting preselected cytosolic particles to each other and to nuclear membrane particles, provided these are located at a distance equal or lower than l_{IF} each from the other.

Cytoskeleton interconnections

The Cytoskeleton interconnections (CI) involved all the IF, MF, and MT networks. A particle of any of these sets is assumed to interact with a particle of any of the two other sets located at an initial distance lower than l_{CI}. These connections are ensured using cables of stiffness k_{CI}. Identically, SF are considered connected to the IF network. This reproduces the indirect connection between the MF and MT with the NM through the IF. In addition, the MF close enough to NM connect to NM directly via CI to reproduce LINC complexes as found in Wakhloo et al. 2020 [Wakhloo2020]. In the same way, the MT centrosome is connected to NM via CI.

The parameters used in this study to define cell model structure are recalled in Tables 1 and 2. They are identical to those used in Vassaux et al. 2019 to calibrate and validate the cell model [Vassaux2019]. The access to the cell model is open at [Vassaux2018].

Structure	MT	IF	MF	SF	NM	IN	CM	CTS	FA
Number	500	200	500	838	648	377	8059	5138	30

Table 1: Number of particles composing each intracellular structure

Structure	k **(nN)**	τ	*l (μm)*	**Source**
MT	228	0	10	[Gittes1993]
IF	157	-0.1	10	[Gittes1993]
MF	10	0.02	10	
SF	45.7	0.2	5	[Deguchi2006]
NM	10	0	<5	
CM	10	0.02	2	
FA	20	0.02	5	
CI	500	0	0.1	

Table 2: stiffness (k), pre-strain (τ), and length (l) values of intracellular cable and spring interactions

2.3 The dynamic substrate

The substrate is an impermeable surface of rigid spherical particles with a radius of 1.66μm that overlap with each other therefore preventing any external particles from sneaking through. The positions of substrate particles are controlled.

The wave motion is generated by moving the substrate particles up and down (Figure 1.a) by imposing their local vertical positions $z(x,n)$ following equation 1, without any horizontal movement. These vertical movements form traveling waves which propagate across the substrate plane.

$$z(x,n) = \frac{h}{2} sin(\frac{2\pi}{\lambda}(x + v_w \,.n)) \quad \textit{(eq.1)}$$

In equation 1, we locally calculate the vertical position of the substrate at the x coordinate along the x axis and the migration iteration of the number n. The sinusoidal waves are defined by the height h, wave length λ, and travel velocity v_w expressed in micrometers per iteration (see Figure 1.c). Thus, $v_w \, . \, n$ represents the total displacement of the traveling wave from the initial cell model position to the current migration iteration number n. Consequently, the topological deformation of the substrate forces the cell model to adapt its shape and respond accordingly.

The substrate particles interact with cell membrane particles via contact interactions, thus preventing the cell from going through the substrate. Focal adhesion particles are positioned on the substrate plane and remain fixed in position during each iteration.

All the simulations started by spreading the cell model on the initially flat substrate until reaching a spread area of 2580µm² and the formation of focal adhesions. Then the substrate was gradually deformed to a corrugated shape before wave travel. This moment represents the starting point of all the videos.

When traveling waves are involved, the deformation travels across the substrate plane. The substrate does not translate horizontally, instead it moves up and down locally to recreate the motion of the waves.

2.4 The process of dynamic curvotaxis in the cell model

Here, we used the same physical mechanisms to model curvotaxis as we did in our previous studies on static substrates [Vassaux2018; Vassaux2019]. Adherent cell migration is driven by many factors. In-vitro experiments showed that curvotaxis appears predominant over other cell migration factors when wave height is 10 µm or greater for a wave length of 100µm [Pieuchot2018; Vassaux2019]. In this study, only the contribution of curvotaxis was included in the cell migration simulations; other factors were not considered. When curvotaxis occurs, we assume that the topography induces a force imbalance on the nucleus between the high force convex area and the low force concave area (Figure 1.b). It consequently becomes harder for the cell to drag its nucleus toward convexities, than to nudge it to concavities. As a result, a bias arises which favors movements toward concave areas. In this study, we considered waves with curvature parameters known to induce a migration bias [Pieuchot2018] that were observed to dominate the steering of cells during migration. The cell model is able to reproduce this bias by predicting the mean displacement of the cells led by the drifting motion of the nucleus. Using the cell model, we predicted how cells would migrate on traveling waves due to dynamic curvotaxis.

The migration of the cell model is an iterative process. Migration is simulated by mimicking a lamellipodium protrusion at the front of the cell and retraction at the rear. A real cell migrates as new FAs are continuously assembled away from existing disassembling adhesions in the direction of motion. While the cytoskeleton connects new FAs, the old ones are disassembled. In the cell model, a single FA is composed of a pair of particles, one active and fixed and the other inactive and mobile as a candidate for a new FA location. The active particle anchors the cell model to the substrate, i.e. it is attached to the moving surface of the substrate and linked to the cytoskeleton of the cell model. Meanwhile, the inactive FA particle moves in the migration direction given by the nucleus offset. The inactive particle then binds to the surface of the substrate and becomes active in its turn: it connects to the cytoskeleton and anchors the cell model to the substrate. The former active particle then becomes the inactive particle. The process is repeated iteratively. In the cellular model, the turnover of an FA is a interplay and a swap between the

fixed active particle and the moving inactive particle. All FAs behave in the same way, with no distinction being made between the front or rear of the cell model. Protrusion at the front of the cell model and retraction at the rear result directly from the curvature-induced nucleus offset that gives direction and magnitude of protrusion and retraction.

More precisely, at the end of each iteration i, the internal displacement of the nucleus $\vec{d}_i$ is computed as the vector directed from the cell barycenter to the nucleus barycenter. At iteration $i+1$, the inactive particles of all the FAs are displaced of $\vec{d}_i$. The cell model migration ends when $\vec{d}_i$ becomes negligible with respect to cell dimensions, when the nucleus has finally stabilized in the middle of the cell model and the model itself has stabilized. The model is not self-excited and does not generate random migration trajectories.

Our study simulates cell migration on traveling waves using an iterative approach. At first, we considered the traveling waves as a sequence of sinusoidal curvatures, with an increasing phase shift between them, thereby accounting for the changing curvature. Subsequently, our iterative migration process involved a sequence of migration steps for the cell model on successive wave profiles, with each profile having a phase shift from the previous iteration. It is worth noting that the extrapolation of our cellular model to the dynamic curvature of traveling waves follows the classical use of the model, which has been previously validated in [Vassaux2019]. By incorporating this validated model, we ensure that our approach is robust and reliable.

2.5 Computational implementation of dynamic curvotaxis in the cell model

To compute the mechanical dynamics of the cell model successively during the migration, each iteration i lasts 0.1s and is subdivided into 1000 sub-iterations of a 0.1ms timestep each.

The travel of the waves is also calculated iteratively. The current wave shape of the substrate is calculated at the beginning of each iteration. From the previous iteration to the current one, the substrate nodes are not repositioned instantaneously. Instead, the total displacement of each substrate node is divided into sub-displacements taking place during 1000 sub-iterations composing the iteration.

Similarly, the nucleus offset due to curvature is measured at the beginning of each iteration to calculate the cell migration displacement. This displacement is then gradually implemented by moving FA nodes during the 1000 sub-iterations. To do so, the total displacement that the FA particles have to travel during an iteration is divided into sub-displacements that are performed during the sub-iterations.

During each sub-iteration, the particles of the substrate and FAs are assigned an appropriate velocity. This velocity multiplied by the sub-iteration timestep results in the sub-displacement. As a result, the particles of the substrate and the FAs move during the sub-iterations and a fortiori during an iteration. This results in a continuous motion of the travelling waves and of the migrating cell model. The substrate, the FAs and the cell move at the same time, in the same timestep and so, the cell model migrates on the moving substrate. Except for FA nodes, cell membrane nodes experience a frictionless contact with the substrate, thus allowing the cell membrane to gradually slide over the moving substrate.

Considering the FA turnover, at the end of each iteration, all the FAs have to reach a new position given by the nucleus offset vector. This final position is reached progressively, as we mentioned earlier, by an interaction between the active and inactive FA particle that occurs at the sub-iteration step. In each sub-

iteration, the inactive FA particle is displaced and becomes active, while the old active particle is detached and becomes the inactive particle that will move in the next sub-iteration.

The calculation of the mechanical state of the cell model at each 0.1ms sub-iteration follows an adaptive iterative scheme ensuring calculation convergence. For the wave speeds we considered in the study, the cell model reached mechanical equilibrium at the end of each 0.1ms sub-iteration. Mechanical computations were achieved using LMGC90 a Non-Smooth Contact Dynamics (NSCD) mechanical solver dedicated to divided medium mechanics [Jean1999; Dubois2016]. Implementing the motion of travelling waves and migrating cell model on a time step of 0.1µs guarantees the convergence of the mechanical calculations at each sub-iteration and the coherence of the entire iterative process of the dynamic simulation of curvotaxis.

Cell migration is here considered as a purely mechanical process without involving duration of biological processes or biochemical kinetics. For instance, cytoskeleton remodeling or focal adhesion creation are instantaneous in the cell model. Computational timesteps were defined only to reach mechanical equilibrium at each sub-iteration. Therefore, the simulation timesteps and biological timesteps are unrelated.

The calculation of the nuclear stress during simulation was carried out using a custom-made post-processing procedure. This procedure accounts for all contact forces external to the nucleus. It also calculates the faceted polyhedron that best represents the shape of the nucleus in order to transfer the external contact forces onto it and calculate the equivalent stress tensor within the nucleus. In our study, the nuclear stress is the hydrostatic pressure derived from the stress tensor.

2.6 Different test conditions

We considered different surface wave profiles all with a wavelength of 100µm which is optimal for observing curvotaxis for a spread cell 60µm in diameter [Pieuchot2018; Vassaux2019].

We varied wave parameters (Figure 1.c) to analyze their influence on dynamic curvotaxis in-silico. We considered the following substrate conditions with different wave propagation speeds given in µm per iteration (µm/it) and constant wave height of 10 µm:

1- “Static” wavy substrate as a reference (speed wave of 0µm/it)
2- “Very slow” traveling waves: 1µm/it
3- “Slow” traveling waves: 2µm/it
4- “Medium speed” traveling waves: 4µm/it
5- “Fast” traveling waves: 8µm/it
6- “Very fast” traveling waves: 16µm/it

We varied the wave amplitude to analyze its influence. We considered the following substrate conditions with constant wave speed of 8 µm/it:

7- “Low” traveling waves: 10 µm high
8- “High” traveling waves: 40 µm high

We analyzed sustained curvotaxis in function of the height and the propagation speed of the waves. We considered the following substrate conditions:

9- "Low & slow" traveling waves: 10 µm high, with a propagation speed of 2 µm/it
10- "Medium height & medium speed" traveling waves: 20 µm high, with a propagation speed of 4 µm/it
11- "Fast & high" traveling waves: 40 µm high, with a propagation speed of 8 µm/it

We analyzed the possibility of directing cell migration by changing the direction of the traveling waves twice:

12- Dynamically changing substrate wave direction

We performed complementary simulations reducing either the diameter of the spread area, the number of focal adhesions, and the actin cortex and stress fibers contractility:

13- Influence of reducing either spread area or focal adhesions, or by altering cytoskeleton on dynamic curvotaxis.

In all simulations the cytoskeleton structure of the cell model which was generated probabilistically as described above is the same. In all simulations, the cell model was dropped at the same midslope point on the wave. As the waves derived from a periodic sine function, stroboscopic effect could occur if the waves moved a distance equal or larger than the wavelength at each iteration. In our study, wave speeds are below this threshold and we can consider that there is no stroboscopic effect in the simulations.

3. Results

3.1 Influence of travelling wave speed

The first result of simulations is that travelling waves both induce and guide cell model migration (Figure 1). Varying the wave speed has an influence on the migration behavior of the cell model (Figure 1.d). For a wave height of 10µm, sustained migration of the cell model is achieved provided the wave speed does not exceed 2µm/it. The wave speed of 2µm/it appears to be the optimal guiding speed over long distances. When the waves travel faster than the optimal speed of 2µm/it, the waves overtake the cell model. However, this does not necessarily prevent migration guidance. Indeed, if the model is overtaken by a wave, it will be pushed by the next wave. For example, although less efficient, at a wave speed of 4µm/it, the cell model can still migrate in the direction the waves travel. This means that wave speeds do not need to be extremely precise to have guiding effect. However, if the waves travel too fast (8 µm/it or above) the cell is not able to migrate properly and cell model guidance is lost (Figure 1.d).

The speed of the cell model depends directly on the speed of the nucleus obtained in the previous iteration. Therefore, in the case of sustained migration, it is normal that both speeds are always equivalent. Above the optimal wave velocity, the simulations show that the cell and nucleus speed diverge (Figure 2). The relative speed of the nucleus fluctuates between iterations, but remains bounded without diverging. Nucleus speed fluctuations increase when the wave goes faster than the cell model.

Simulation of cell migration on a 10µm-height "static" wave with a propagation speed of 0 µm/it shows little net cell displacement, which corresponds to only a small repositioning of the cell model closest to the concave region of the wave trough (Figure 2.a). This repositioning of the cell model is associated with a mechanical relaxation of the nucleus as indicated by the asymptotic decrease of nucleus stress towards the residual stress of ~1kPa after the mechanical relaxation of the cell structure (Figure 3). In contrast, mechanical relaxation of the nucleus is slower or prevented altogether in scenarios where the cell model is subjected to faster moving waves of the same height. When the waves propagate at a speed greater than the optimal 2µm/it and overtake the cell model, periodic loading of the nucleus can be observed with higher levels of peak and average stress.

3.2 Influence of traveling wave amplitude

With a wave height of 10µm cell model is not able to keep up with waves propagating at 8 µm/it (Figure 1.e). However, when wave heights are increased to 40 µm, the cell can sustain curvotaxis without being overtaken by the waves (Figure 1.d). At a wave speed of 4µm/it, sustained migration of the cell model requires a wave height of 20µm (Figure 1.f). So, the cell model can undergo sustained and reliable curvotaxis at higher speeds when wave heights are increased, and as a result, the cell can travel greater distances in the same amount of time (figure 4.a). We identified an optimal pairing of wave speed (WS) and wave height (H) to produced sustained migration guidance: (WS=2µm/it, 10µm); (WS=4µm/it, 20µm); (WS=8µm/it, 40µm). Although the wave velocity remains constant during the simulation, when the wave speed and height are higher, the speed of the cell model as well as the relative speed of the nucleus appear to be more dynamic and irregular, varying slightly around their mean value, with short phases of acceleration and deceleration (Figure 4). The higher the wave, the lower the nucleus stress (Figure 5). In addition, we observe that the cell model is better able to center itself in the valleys of 40µm-height waves that result in lower stress on the nucleus. The traction force exerted by the cell model on the substrate also decreases as wave height increases (Figure 5d). Traction force was defined as the sum of all the forces, in terms of magnitude, that the cell exerts on the substrate via all its FAs. Interestingly, high waves allow sustained migration at higher speeds with lower nucleus stress and lower cell contractility.

To better understand how traveling wave curvature may influence cell migration speed, we simulated cell model migration on 3 static wave profiles (non-travelling) of 10, 20, and 40µm in height. In each case, the cell model was initially located in the middle of the slope of the static wave. On static waves of 10, 20, and 40µm in height, we reported that the speeds of the cell model at the first iteration of migration were 2.12µm/it; 4.29µm/it, and 8.36µm/it respectively. These speed values are strongly correlated with the curvature gradients of the static waves, since we obtain a linear relationship between them (Figure 6). The migration speeds of cell model on static waves are very close than the optimal traveling wave speeds, 2µm/it, 4µm/it, and 8µm/it, that were found to guarantee sustained cell migration on waves 10, 20, and 40µm in height respectively (Table 4). By simulating cell migration on traveling waves, we found that the optimal wave speed is the maximal speed of the waves that the cell model is able to follow in a sustained way. Here, by simulating cell model migration on a static wave profile, we deduced that the optimal wave speed is equal to the speed of the cell model as it migrates on the static profile of the wave. This value

depends only on the intrinsic mechanical properties of the cell model and on the wave topography. So, the optimal wave speed value highlights the intrinsic capability and dynamics of the cell model to migrate on a given wave pattern. For a given wave pattern and a given set of cell model parameters, the expected optimal wave speed would be given by the curvature gradient between tops and troughs of waves. The curvature gradient of sinusoidal waves is related to the wave slope. Therefore, wave slope could also be used as a simpler indicator for the wave in order to define optimal wave speed.

Wave height (µm)	Cell speed on static wave (µm/it)	Optimal wave speed for sustained cell migration (µm/it)
10	2.12	2
20	4.29	4
40	8.36	8

Table 4: Comparing cell speed on static substrate vs optimal travelling wave speeds allowing sustained cell migration

3.3 Influence of cell mechanical properties

We simulated structural changes in the cell model by mimicking different states for adherent cells or the knockdown of some intrinsic cell structure. We analyzed the contribution of these cell properties in curvotaxis when the model is subjected to a 10 µm high static wave (Figure 7). The reduction of the number of focal adhesions, the diameter of spread cell area, or the stiffness of actin cortex and stress fibers all result in the decrease in cell contractility. The nucleus is then less stressed and the nucleus offset decreases. As a result, the nucleus-oriented cell migration is impaired.

Moreover, when the model is less contractile than the control, the model stabilizes further from the concave wave trough. The loss of structural integrity of the cell model increases the wave trough targeting error. The model becomes slower and less accurate. In Figure 7.c, we defined and reported the quantity (1 – concave-targeting error) that we considered equivalent to the precision of targeting concave area spatially.

If we cross these two phenomena and multiply the speed of the nucleus by the precision of the targeting concave, we obtain the current sensitivity of the cell model to dynamic curvotaxis (Figure 7.d). The results clearly indicate that the sensitivity to dynamic curvotaxis depends on the structural integrity of the cell model.

3.4 Steering cell migration dynamically by changing the direction of propagating waves

We started the simulation by generating unidirectional traveling waves at the surface of the substrate. Then during the simulation, we changed the direction the waves traveled by 90°, which prompted the cell model to adapt its direction of migration. We changed the direction in which the waves propagated again and observed that the cellular model again adapted its trajectory (Supplementary Movie 1). We conclude that the cell model can dynamically adapt its trajectory.

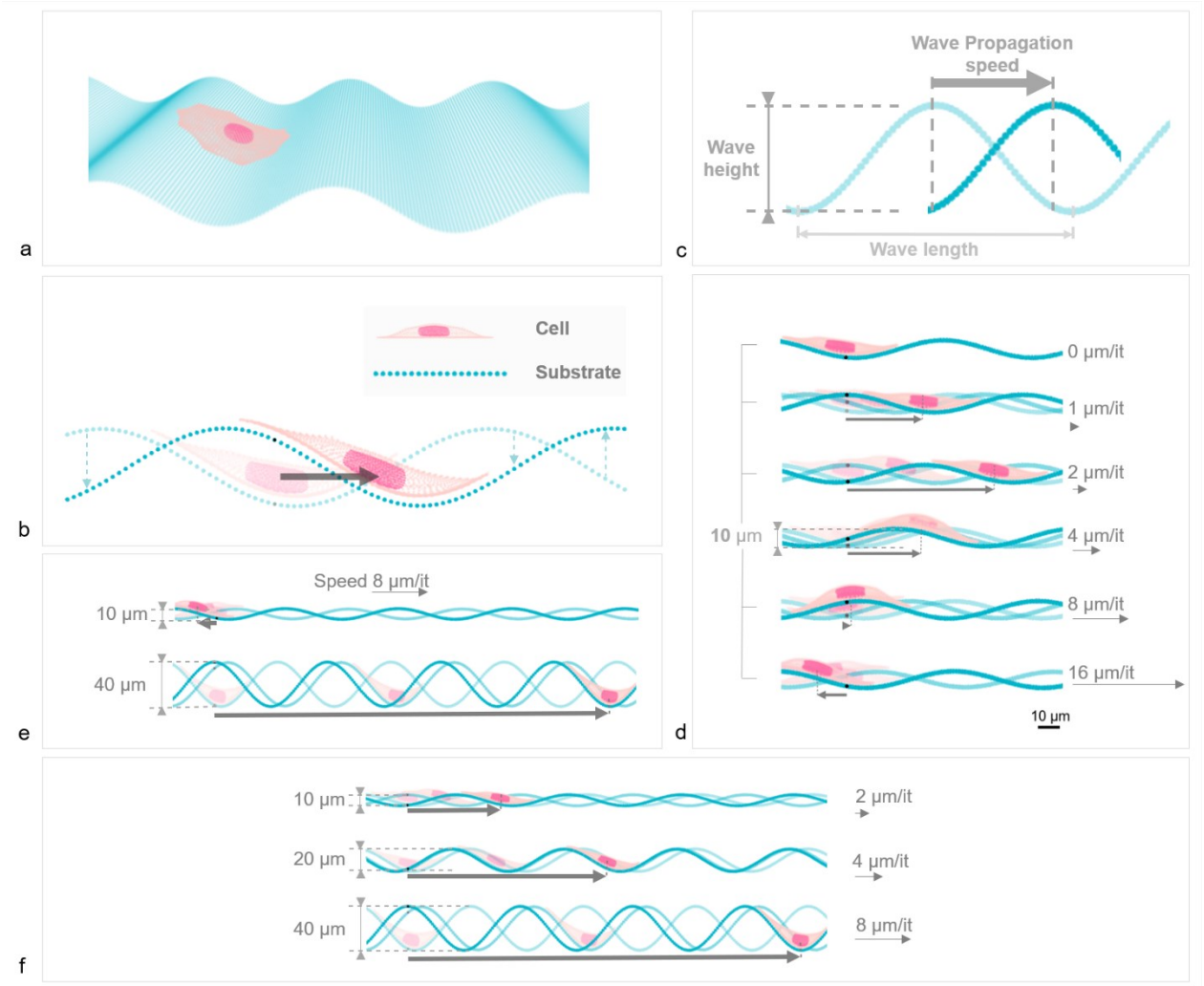

Figure 1: Cell model (salmon) and the nucleus (pink) on traveling waves (turquoise). The waves propagate horizontally along a single axis by making the local surface move up and down. As the wave moves, so does the concavity (valley). Subject to curvotaxis, the cell model is prone to migrate toward concavities. As a result, the cell model moves over the surface of the substrate as it continuously seeks the closest valley. (b-f) are side views. a) Sky view of a cell avatar on the undulated substrate (Supplementary Movie 1). b) The surface of the substrate is defined by a set of individual contact spheres (drawn smaller to identify them individually). These substrate spheres are fixed horizontally, in contrast, their vertical movement generates the traveling wave pattern. As the wave travels, so does the concavity (valley), which in turn attracts the cell model (Supplementary Movie 2). c) The propagating waves are parametrically defined by their wave lengths (100 µm), while their height varies between conditions (10 µm, 20 µm, 40 µm), and their horizontally uniaxial propagation defined in µm/iteration (µm/it) (one iteration corresponds to a computational time of 0.1s). d) The total distance traveled by the cell model is compared based on different wave propagation speeds for identical wave heights of 10 µm (Supplementary Movie 3). e) Cell model was placed on substrates with identical wave propagation speeds, however, different wave heights lead to different outcomes. f) Sustained curvotaxis achieved at different speeds, based on different wave heights (Supplementary Movie 4).

WS=0µm/it WS=1µm/it WS=2µm/it WS=4µm/it WS=8µm/it WS=16µm/it

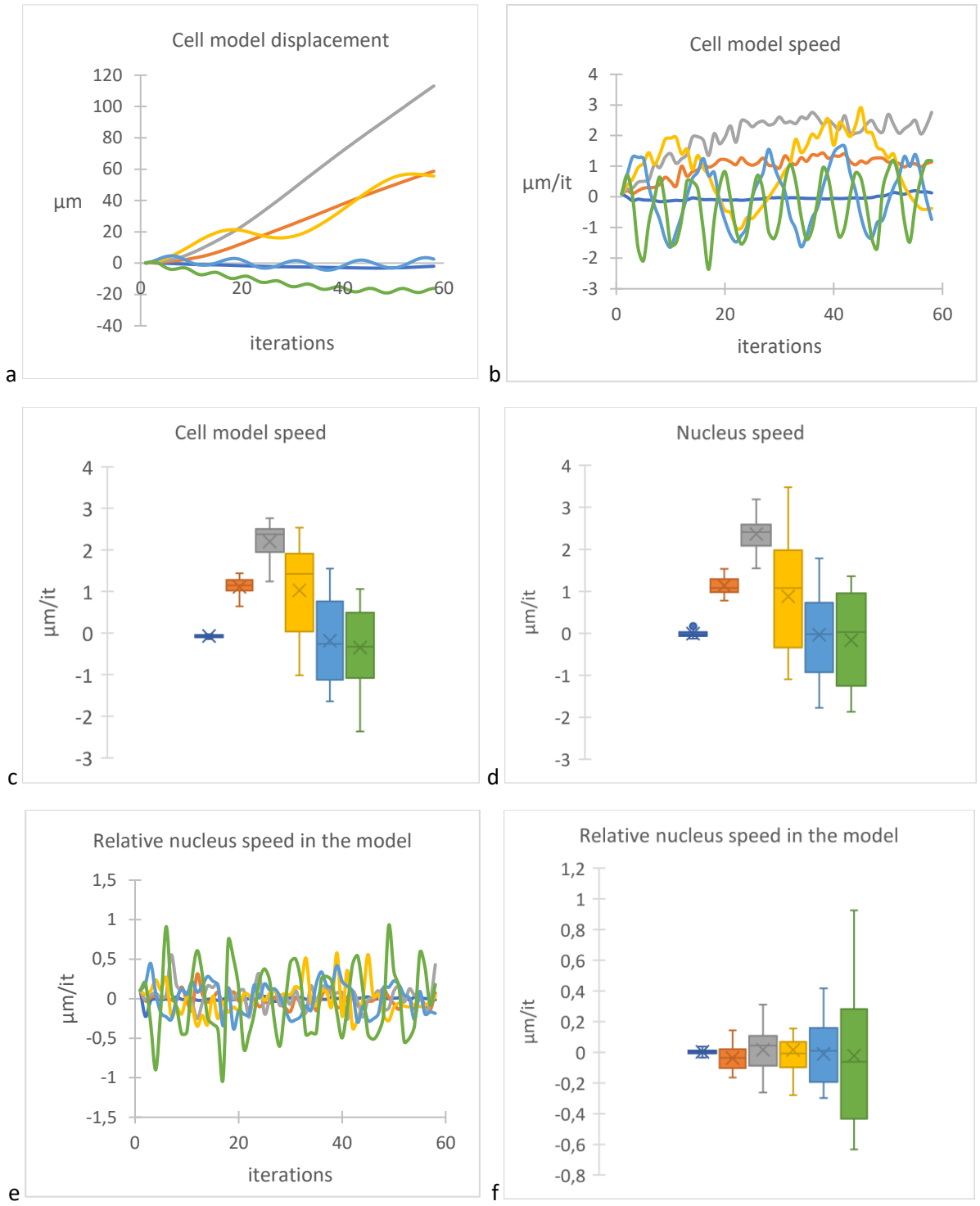

Figure 2: Simulation results of single cell migration induced by 10µm-height waves of various wave speeds (WS). WS conditions are each represented by a specific color a) Instantaneous distance traveled depending on wave speed. Each curve represents only one simulation. b) Instantaneous cell speed depending on wave speed. c) Box plot of cell speed. Box plot represents the distribution of cell speed by indicating the min and the max and the lower and upper quartiles. Each box plot represents only one simulation between the 20th and the 60th iteration, during which the migration regime of the cell model is stabilized. d) Box plot

of nucleus speed depending on wave speed. Instantaneous (e) and box plot of the (f) relative speed of the nucleus inside the cell during the simulations. The box plots are defined using the values acquired during the iterations between the 20th and the 60th, during which the migration regime of the cell model is stabilized.

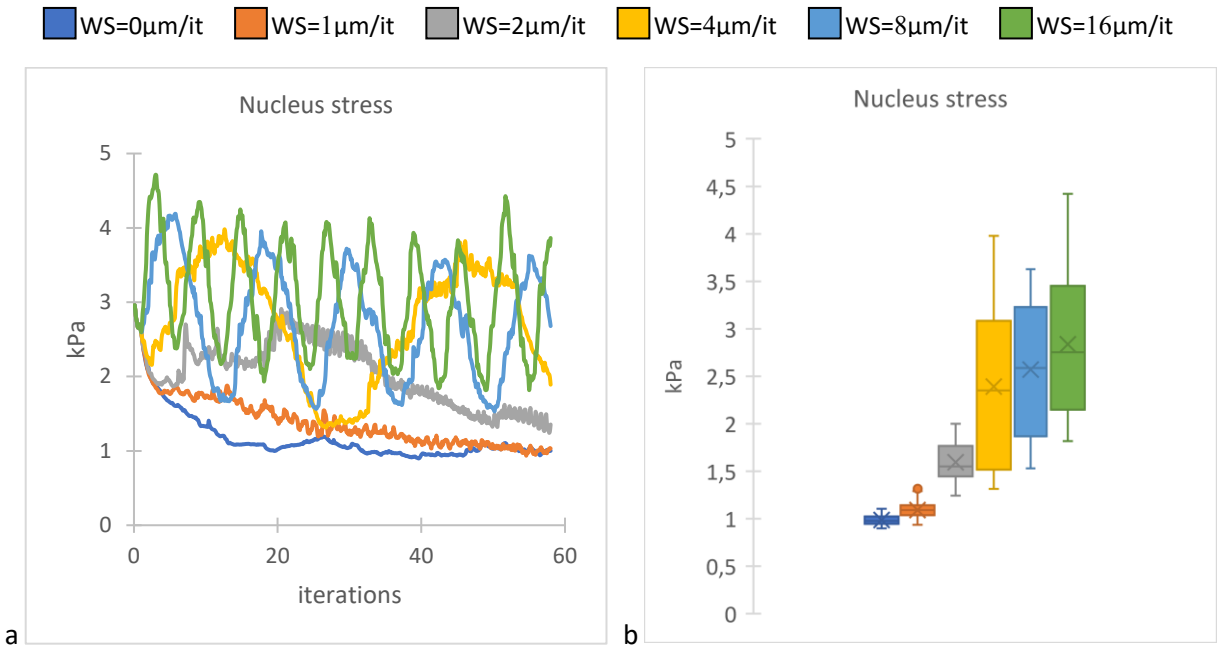

Figure 3: Simulation results of cell model subject to 10 µm high traveling waves of various wave speeds (WS). Each WS condition has a specific color. a) Instantaneous compressive stress on nucleus. b) Box-plot representation of compressive stresses on the nucleus acquired during the iterations between the 20th and the 60th, during which the migration regime of the cell model is stabilized.

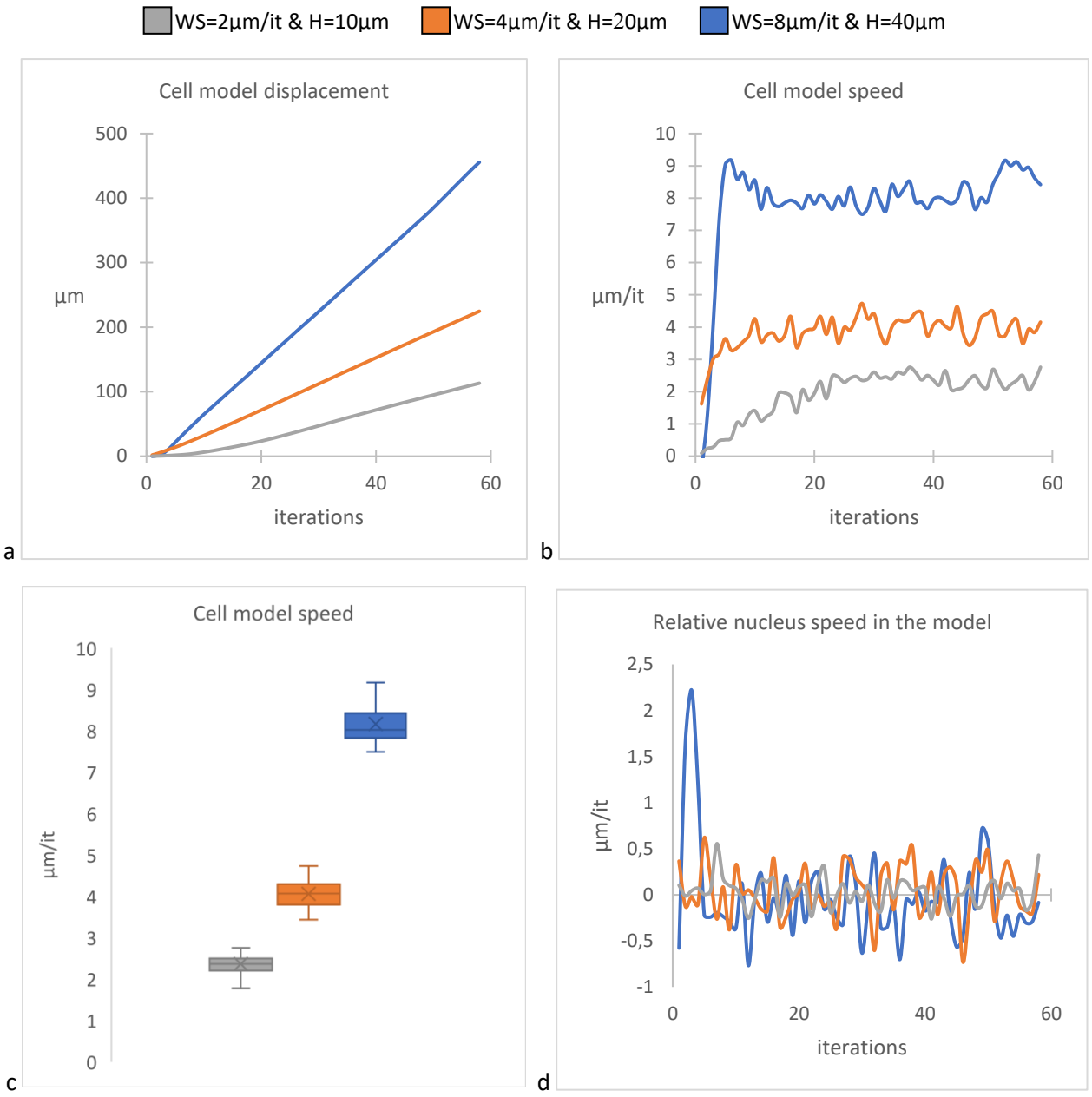

Figure 4: Simulation results of cell migration induced by traveling waves depending on wave heights and speeds. Wave speed (WS) = 2µm/it, Height (H) =10µm; WS=4µm/it, H=20µm; WS=8µm/it, H=40µm. a) Distance traveled from origin. b) Migration speed. c) Box plot of cell speed obtained during stationary regimes of cell model migration defined between iterations 20-60. d) Relative speed of the nucleus movement inside the cell. WS=wave speed; H= wave height.

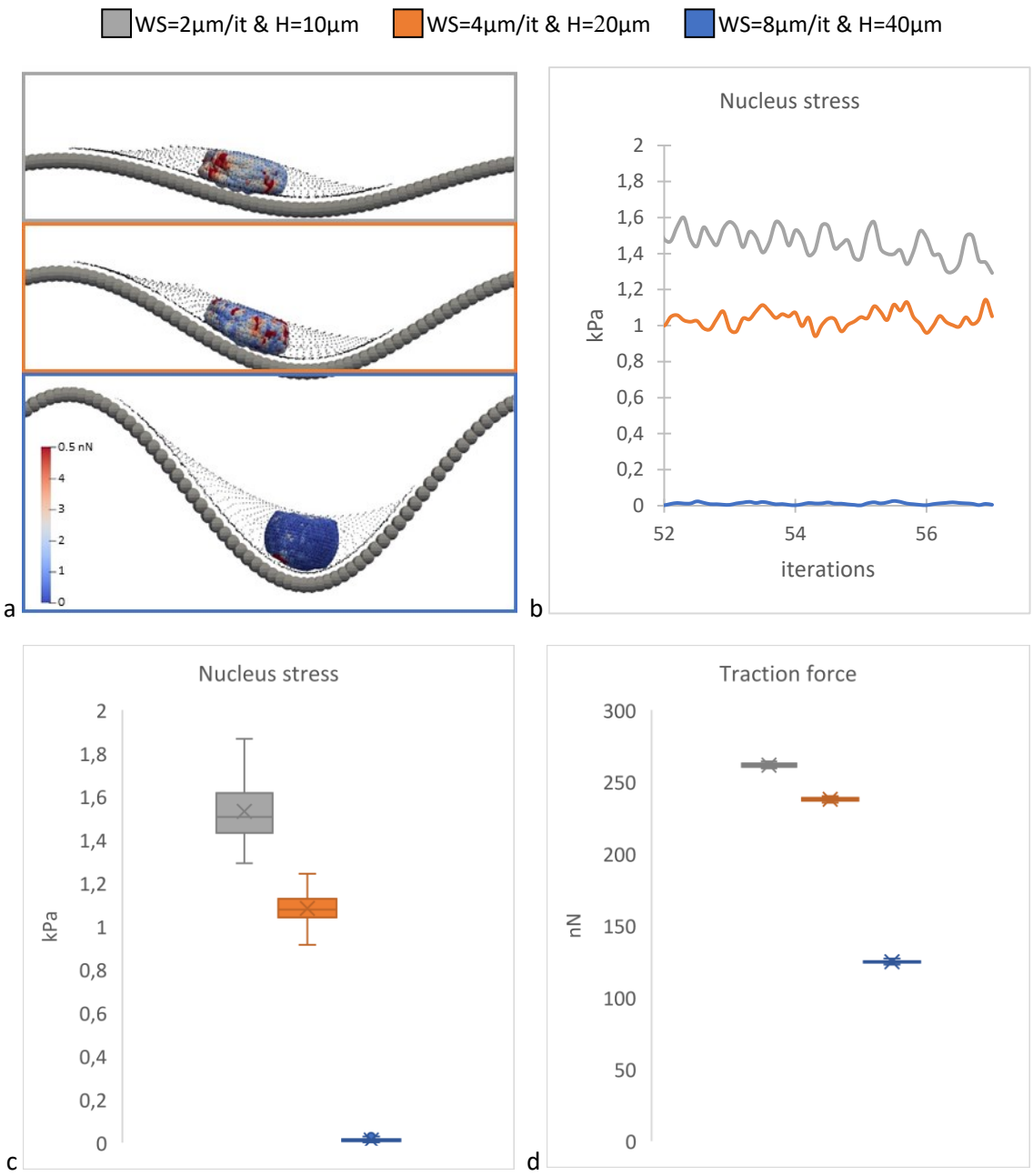

Figure 5: Nuclear stress and magnitude of traction force exerted by the cell on the substrate via all of its focal adhesion on traveling waves of optimal speed and height. Wave speed (WS) = 2µm/it, Height (H) =10µm; WS=4µm/it, H=20µm; WS=8µm/it, H=40µm. a) 3D view of the nuclei on traveling waves of optimal height and speed. The particles, constituting the nucleus membrane, are colored as a function of the amplitude of the local cohesion forces. Instantaneous (b) and box plot of (c) compressive nuclear stress. d) box plot traction forces exerted by the cell on the substrate as it migrates. Box plot values are obtained during the stationary regime of cell model migration observed between 20-60 iterations. WS=wave speed; H= wave height.

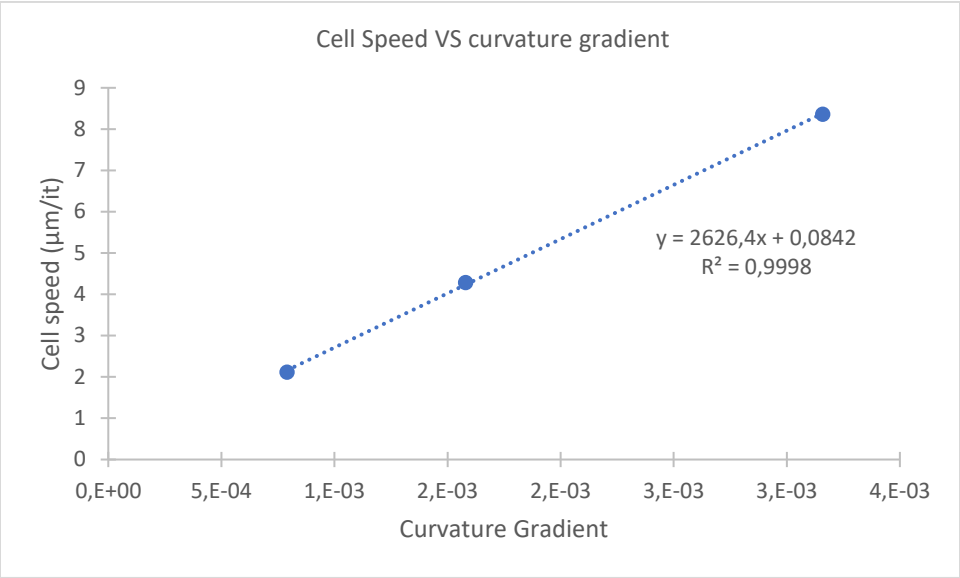

Figure 6: The speed of cell model migration depends on the curvature gradient of the wave. We simulated cell model migration on 3 static wave profiles of 10, 20, and 40µm height. In each case, the cell model was initially located in the middle of the slope of the static wave. We reported the speeds of the cell model that occurred during the first iteration of migration, that is, 2.1µm/it, 4.3µm/it and 8.4µm/it, respectively.

Curvature gradient was calculated between the top and the trough of the wave as $\frac{\Delta C(x)}{\frac{1}{2}WL} = 8\frac{H.\pi^2}{WL^3}$, with H the height of the wave between top and trough, WL, the wave length of undulation and the curvature, $C(x) = f''(x).(1 + f'(x)^2)^{-\frac{3}{2}}$ with f(x), the equation of the wave.

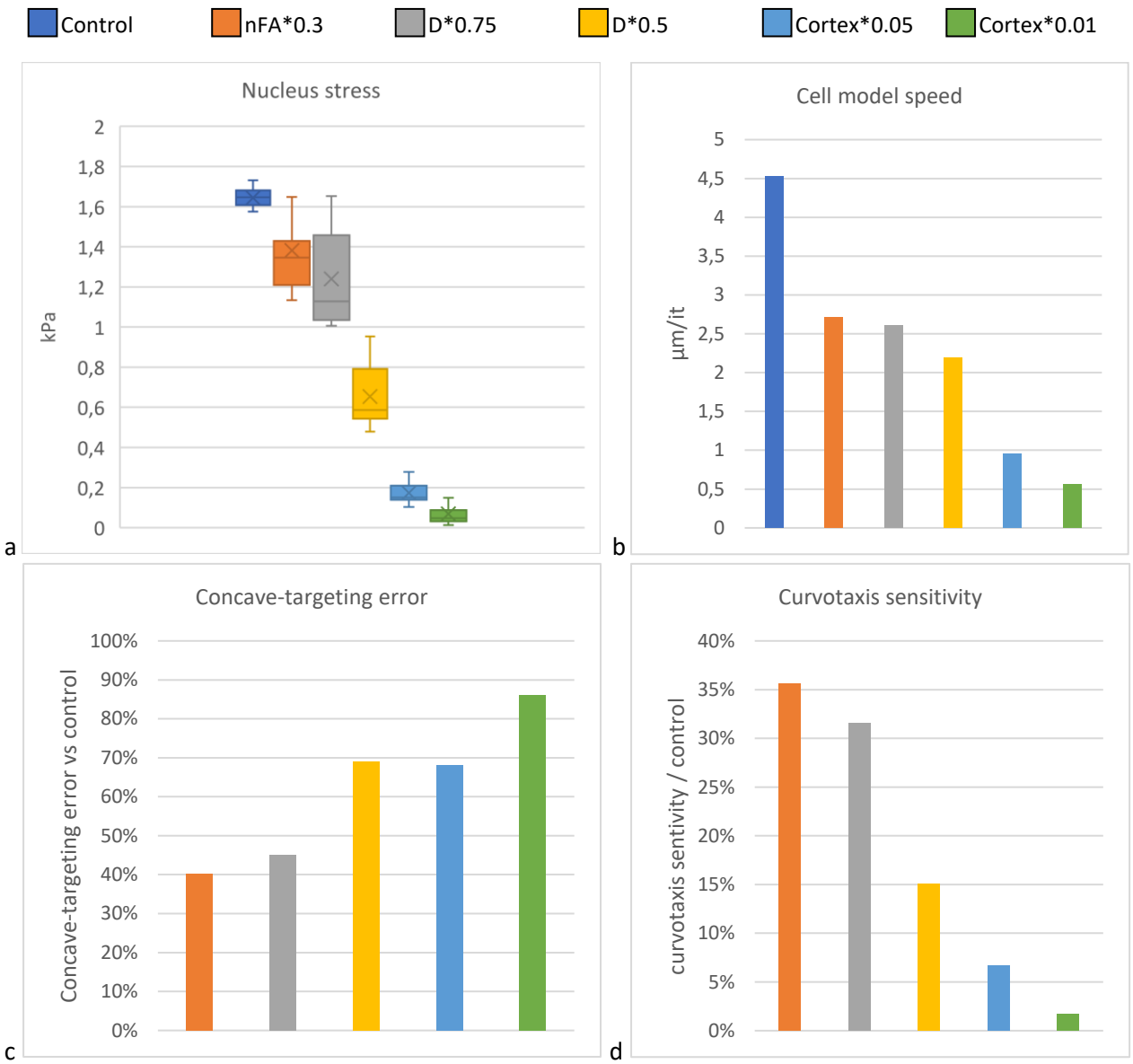

Figure 7: Structural changes in the cell model and their influence on the sensitivity to curvotaxis when the model is subjected to a 10 µm high static wave. Alternately, the number of focal adhesions (nFA) was multiplied by 0.3, the diameter of the spread cell by 0.75 or 0.5, the stiffness of the actin cortex and the stress fibers by 0.05 or 0.01. Each of these conditions has been given a specific color in the graphs. a) Box-plot representation of compressive stresses on the nucleus acquired during the migration of the cell model on the static wave from the start and until it stopped at the concave area or at its vicinity. b) Average nucleus motion speed in the cell model towards the concave region of the static wave trough. c) Concave-targeting error vs control. When the cell model stopped near the concave area, we measured the distance between the center of the cell model and the center of the concave area. This distance, normalized by half the wavelength of the wave, defines the Concave-targeting error. The concave-targeting error vs control is the relative concave-targeting error committed by an altered model compared with the error committed by the control model. d) Curvotaxis sensitivity calculated as the nucleus speed in (b) multiplied by (1 – concave targeting error in (c)), the (1 – concave-targeting error) being equivalent to the chances of targeting concave area spatially.

4. Discussion

The results of the model suggest that dynamic substrate curvature can be used to guide cell migration over long distances. This finding may have a profound impact on the way we apprehend single and multi-cell migration. In the end, these findings may trigger new ways to tackle and explain a plethora of phenomena in developmental biology and tissue engineering.

However, by themselves the results of the model are not sufficient to fully describe the essential characteristics of a future dynamic substrate. First, in the model, the speed of the traveling waves was not described in physical units, therefore quantitative estimates will require additional analysis. Secondly, although curvotaxis is known to impact cell migration, in some cases its influence is non-deterministic. In other words, cell migration remains partially random which was not considered by the model. We will address both of these dilemmas below.

4.1 Estimating the speed of the traveling waves

Estimating optimal speed for traveling waves must be relative to the capability of the cells to migrate spatially under dynamic curvature gradient. The maximal speed of the traveling wave is given by the threshold below which the cells can maintain cell migration guidance and above which they cannot do so.

Based on previous studies [Pieuchot2018], for a wave height of 10 µm, we observe that mesenchymal stem cells can generally migrate at about 20 µm/h and up to 40 µm/h. We therefore conclude that traveling waves should propagate slower than 20 µm/h to allow all cells to keep up. Otherwise, we expect that some cells would be overtaken by the waves, if the waves traveled faster than 20 µm/h, which would be less efficient as the simulation results show.

4.2 Ensuring reliable migration

Pieuchot et al. showed that nucleus positioning and cell migration were strongly influenced by static waves with a height of 10 µm and a wave length of 100 µm, this phenomenon being coined curvotaxis [Pieuchot2018]. Moreover, Pieuchot et al 2018 also showed that actomyosin contractility and nucleus integrity were necessary for curvotaxis to occur. Later Vassaux et al 2019 created a numerical cell model that successfully reproduced curvotaxis. The hypothesis was that substrate curvature influence nucleus positioning and that the cell would then reposition its adhesions to center its nucleus. Simulation results show that cells could migrate to concave area, while avoiding convex peaks.

In the current model, the effects of curvotaxis were the only contributors to cell migration. This study was thus conducted at the detriment of common migration pathways. Generally, in adherent cells, protrusion and migration are driven by complex interplay between adhesion binding and unbinding, actin polymerization, actomyosin contractility, and mechanosensitive signaling. These primary contributors to cell migration would have a major impact on simulation results, and taking them into account would thus better match expected experimental results. This suggests that curvotaxis should only be considered as a secondary contributor to cell migration that may bias cell directionality. Indeed, with the limited curvature generated by low waves (less than 10 µm high), curvotaxis contributes to cell migration, but it is not dominant. As a result, curvotaxis has a probabilistic effect on cell migration.

However, the pronounced curvature of high waves significantly increases the guiding effect of curvotaxis [Pieuchot2018; Vassaux2019], to the point that it can become dominant. At that stage, cells seldom go over convex summits [Pieuchot2018] when wave heights are 10 µm or higher. In other words, being able

to generate waves that are at least 10 µm high should reliably promote and guide cell migration. Common contributors to cell migration may consequently become negligible in a high curvature context. This is why our study only focuses on the effect of curvotaxis.

The linear relationship between the cell speed and the height of the waves, showed in Figure 6 was not verified experimentally in [Pieuchot2018]. Pieuchot et al 2018 only observed that the cells travel on average two times faster when they were in convex area than when they were in concave areas. Nonetheless, one expects the cell speed to be bounded and not to increase indefinitely with curvature gradient and wave height.

4.3 Substrate specifications defined by the model

We have estimated an appropriate wave speed of 20 µm/h and wave heights of 10 µm to induce reliable cell migration over long distances and showed promising biological examples [Sokolow2012, Jaffe1998, Jaffe2008]. We can define the specifications of a functional substrate. Based on our results, we predict that reliable and sustained migration can be achieved by generating traveling waves with:

- wavelengths of 100 µm
- heights between 10 and 40 µm
- travel speeds ranging from 10 to 20 µm/h.

This low wave height substrate would consequently generate waves with frequencies ranging from 0.03mHz to 0.06mHz. On the other hand, on strongly curved substrates [Pieuchot2018], speeds up to 40 µm/h may temporarily be achieved to the detriment of reliability.

According to the model, our study shows that cells can surf travelling waves provided that the waves travel slower than the cells. The model also predicts more subtle behaviors depending of wave patterns such that:

- Cells can surf faster if the wave height is increased. However, this result is dependent on the hypothesis assuming that curvotaxis is a phenomenon involving only nucleus stress and cell repositioning leading to its mechanical relaxation.
- Cells can still move over long distances even if they are overtaken by waves that travel a little bit faster than the cell. Interestingly, this implies that propagation speeds do not need to be extremely precise to have an effect.
- Nuclear deformation is lower when wave height is increased. This difference in nuclear deformation could also be physiologically relevant as it may alter the mechanobiological response of the cell.

4.4 Comparing our in-silico results with existing biological observations

In 2019, Tomba et al. cultured cells on a dynamic substrate capable of switching from a flat to a wavy state [Tomba2019]. Initially, the substrate, a PDMS film, was stretched to 100% and then laser irradiated. When the substrate was relaxed, wrinkles of ~15µm height and ~40µm wavelength were formed. The top and bottom of the wrinkles are distant by 20µm from each other in the horizontal direction. Saos-2 cells were cultured on the flat substrate stretched to 100%. When the substrate was relaxed and wrinkles formed, the cells migrated towards the concave valleys within about 2 hours. This indicates that the cells can

migrate a horizontal distance of 20µm in ~2h, at a speed of ~10µm/h to reach the nearest valley. While the guidance of cell migration by dynamic curvotaxis over long distances has not yet been studied experimentally, the study by Tomba et al. in 2019 can be considered as the first step towards an in vitro proof of concept of dynamic curvotaxis, since cells migrate to the concave areas when a vertical undulation suddenly appears. Cells are able to dynamically detect a change in curvature. Undulation of the substrate induces the migration of cells over very short distances, migrating away from convex peaks to reach concave valleys [Tomba2019]. Moreover, the cell migration speed we estimated on the basis of our traveling wave simulations is consistent with the experimentally measured cell migration speed. Therefore, we are able to consider that the study of Tomba et al. supports our study in terms of concept and final results experimentally.

The examples selected from the literature and stated in the Introduction all include mention of naturally occurring curvatures induced by ultraslow calcium waves. During development, various ultraslow calcium waves travel at 3 to 60 µm/h, making such waves plausible inducers of dynamic curvotaxis [Jaffe1998; Jaffe2008]. Our simulation results show that effective migration can be induced by waves traveling at optimum speeds of 20 µm/h when wave heights are low. With a wavelength of 100 µm, this speed corresponds to a wave frequency of 0.06mHz. In drosophila, Sokolow et al. 2012 found the contraction waves responsible for cell ingression belonged to the frequency band ranging from 0.01 to 0.1mHz, this suggests a possible adequation [Sokolow2012]. This sub-millihertz frequency range was observed by measuring the fluctuation in apical cross-sectional cell area during embryo development. Although we cannot directly relate these results in terms of wave height since the cells are not laying on a 2D plane that deforms along its perpendicular axis. Slow contractions can therefore promote cell ingression and sorting. These experimental observations suggest that folds and furrows that are induced by ultraslow calcium waves would form and propagate at speeds that closely match those found by the model. Our results can be considered consistent with these biological examples.

4.5 Consistency of cell model extrapolation to dynamic curvature case

Here, we extrapolated the domain of application of our model from the case of static curvatures [Vassaux2019] to the case of dynamic curvature. Our model was originally developed and validated on and for static curvatures, nonetheless we consider that this extrapolation to the dynamic case is relevant. The intrinsic mechanism of curvotaxis has been defined as cell migration guidance by the nucleus offset induced by curvature gradient [Vassaux2019]. In the present study the intrinsic mechanism of curvotaxis remains the same. The only difference between static curvotaxis simulations and dynamic curvotaxis simulations is the slightly motion of the substrate under the migrating cell model. In dynamic curvotaxis simulation, the motion of the travelling waves and the migrating cell model is computed by considering sub-iterations with a time step of 0.1µs. During such a time steps, the speed and displacement remain very low.

The advantage of considering dynamic curvotaxis and displacement wave generation, as we have done in the present study, is the maintenance of cell migration guidance. Indeed, when the wave speed matches the speed of the cell model, the cell model is continuously exposed to the same curvature gradient despite the fact that the cell model is moving. This constantly maintains the same level of mechanical tension in the cell model and the same nucleus offset between simulation iterations.

So, the extended application domain of the cell model to the dynamic curvature of traveling waves implies a use of the model following and respecting the classical use of the model validated in [Vassaux2019]. Thus, we may consider that our present results are consistent with our previous study.

4.6 Physical interpretation of the cell model on travelling waves

The cell model on moving curvature can be likened to a system subject to mechanical potential energy, biased cell migration, and mechanical relaxation. For a fixed curvature, this system has maximum potential energy when it is at the most convex point, at top of the wave. This potential energy induces a bias in cell model migration until the cell model reaches the concave region, where it relaxes. Then, the structural reorganization of the cytoskeleton with a more rounded cell shape leads to a mechanical relaxation of the system. The time taken to reach the concave region could be assimilated to a relaxation time. The speed of the cell model to reach concavity could be assimilated to an intrinsic relaxation speed. This speed defines a threshold speed.

The generation of a travelling wave will constantly provide potential energy to the system to prevent complete mechanical relaxation. Below the threshold speed, the cellular model surfs the wave. Above the threshold speed, the cell model is overtaken by the wave. In this case, the cell model and its nucleus undergo an oscillating mechanical stress, the stress being high when the cell model is overtaken by the top of the wave. The frequency of oscillating stress is the same as that of the overtaking of the cell model by the wave. However, further work is needed to propose an analytical model able to discriminate the different regimes of the cell model on travelling waves, from guided migration to no migration accompanied by fluctuating intracellular mechanical stresses.

It is worth mentioning that the wave speeds studied here were slow enough such that the inertia of the cell model remained marginal. The particles in the cell model have the same density as water and the inertial forces are weak compared with the mechanical interaction forces that reproduce the contractile cytoskeleton.

4.7 Limits of this study

The cell model we used in this study does not reproduce the dynamics of the cell migration mechanism which results from complex interplay between adhesion binding/unbinding, actin polymerization, actomyosin contractility, and mechanosensitive signaling. Each of these elements can be influenced by a dynamic change in curvature. In the present study, the representation of the cell migration mechanism is very rudimentary. We only reproduce the protrusion of the lamellipodium at the front of the cell and a limited remodeling of the cytoskeleton at the front and rear. Indeed, we do not attempt to analyze the possible influence of dynamic curvature on the dynamics of each element of the cell migration mechanism. Instead, we analyze the influence of dynamic curvature on the mechanical positioning of the cell nucleus, which has been shown to bias the migration direction on static curved substrates. In this study, we considered that dynamic curvotaxis is driven by the mechanical relaxation of the cell in the direction of motion of the nucleus pushed towards the concave trough of traveling waves.

Although, we believe that this simplified cell model is able to reproduce the general migration bias that cells will experience when subject to travelling wave, in its current state the model does not represent the probabilistic trajectories that cells would normally generate. For example, cells were shown to migrate in the same direction the wave travel at, however, in-vitro experiments will most likely show that cells also travel in part perpendicularly to the waves.

The authors who have developed phase-field models propose a dynamic representation of the cell migration mechanism [Marzban2019; Winkler2019]. They also show that curvature influences cell migration by proposing a mechanism other than the one we modeled. The results of phase-field model simulations indicate that static curvature can also influence the flow of intracellular actin through which the cell polarizes.

In the future, we wish to integrate the dynamics of focal adhesions and cytoskeletal remodeling more accurately. It would also be interesting in the short term to confront these two types of modeling, as well as others, on dynamic substrates and on the traveling waves we considered here. It is possible that dynamic curvotaxis results from competition or cooperation between different curvature sensitivity mechanisms.

4.8 Perspectives and applications

Once confirmed experimentally by testing cell migration on dynamically curved substrates, we believe that dynamic curvotaxis may significantly impact our understanding of cell mobility. Not only will it become an additional phenomenon to consider when trying to explain single cell motility, such as ingression, but we expect that dynamic curvotaxis may also have a profound impact on our understanding of collective cell migration and the behavior of cell groups. Several examples have demonstrated that for collective cell migration to emerge, various phenomena have to work in synergy, otherwise the collective behavior becomes undefined [Mayor2016; Shellard2019; Szabó2016]. Therefore, it is reasonable to assume that dynamic curvotaxis may be one of the key phenomena required to explain several processes involving collective cell migration and controlled tissue growth [Rougerie2020]. As a result, in addition to dynamic curvotaxis, dynamic curvature may have a significant impact on embryogenesis, regeneration, and cancer metastasis.

We propose to experimental scientists travelling wave heights and speeds to guide cell migration. Important technical development is still needed to design dynamic substrates. Dynamic environments would enable groundbreaking in vitro cell analyses to be carried out by mimicking in vivo conditions, and could have industrial applications in cell and tissue engineering involving the guidance of migration over long distances, the mechanical stimulation of cells, and the sorting of cells into those that respond to curvature and those that do not. We also believe that more elaborate wave shapes, such as a crescent shape, would better constrain cell movements and thus prevent cells from moving perpendicular to the intended direction, a phenomenon we have not modelled but which we expect to occur experimentally.

Interestingly, up to now most models of cell migration with a strong emphasis on cell mechanics have been used only to explain known experimental results. At this time, in our field, it is still rare to use a model as a predictive tool to both engineer experiments and estimate their outcome. Although only experimentation will tell whether our forecast is valid, we nonetheless believe that predictive cell modeling is the future.

Conclusion

Cell migration is influenced by curvature, but the effects of dynamic curvature have not been shown at this time. While there are numerous examples of folds, furrows, and invaginations that induce dynamic changes in curvature during embryo development, dynamic substrates able to promote cell migration do not exist at the moment. For this reason, we used a numerical model to predict how deformation waves traveling at the surface of a substrate could promote long distance cell migration. The results of the model suggest that dynamic substrate curvature defined by traveling waves can be used to guide cell migration over long distances. Although curvature is generally considered as a statistical migration bias, in this study we purposefully chose wave heights that appear to make this bias dominant over other parameters that would otherwise influence cell migration trajectories. Our study shows that wave height and travelling wave speed of the wave are key. A speed higher than the optimal speed would result in poorer or no cell

migration. Although, due to technical limitations, currently it is not possible to validate our results experimentally, we anticipate that validation and our results are consistent with the existing literature.

Based on our analysis we propose the following substrate specifications to achieve migration experimentally: the wave should have a wavelength of 100 µm, a height of at least 10 µm, and propagate at 10 to 20 µm/h. The model also predicts that increasing the wave height should allow for efficient migration for higher travelling wave speeds.

Authors Contributions

I.M., J.L.M, wrote the main manuscript text with substantial contributions from G.C., M.V., L.P, V.L and K.A.

I.M., J.L.M., M.V., G.C. and D.L. prepared and launched the in-silico simulations. I.M. prepared the Figure 1 and J.L.M. the others. All authors reviewed the manuscript.

Competing interests

The authors declare no competing interests.

Data availability

The datasets related to the codes that we used to generate the cell model and to launch cell migration simulations for the current study are available via the following persistent web link: https://amubox.univ-amu.fr/s/bKiWG6r87nazLP8.

The large datasets of computational results that we obtained during the simulations and we analyzed for the current study are available from the corresponding author on reasonable request.

References

[Arima2011] S. Arima, K. Nishiyama, T. Ko, Y. Arima, Y. Hakozaki, K. Sugihara, H. Koseki, Y. Uchijima, Y. Kurihara, H. Kurihara, Angiogenic morphogenesis driven by dynamic and heterogeneous collective endothelial cell movement, Dev. Camb. Engl. 138 (2011) 4763–4776. https://doi.org/10.1242/dev.068023

[Bailles2019] A. Bailles, C. Collinet, J.-M. Philippe, P.-F. Lenne, E. Munro, T. Lecuit, Genetic induction and mechano-chemical propagation of a morphogenetic wave, Nature. 572 (2019) 467–473. https://doi.org/10.1038/s41586-019-1492-9

[Caballero2015a] D. Caballero, R. Voituriez, D. Riveline, The cell ratchet: Interplay between efficient protrusions and adhesion determines cell motion, Cell Adhes. Migr. 9 (2015) 327–334. https://doi.org/10.1080/19336918.2015.1061865

[Caballero2015b] D. Caballero, J. Comelles, M. Piel, R. Voituriez, D. Riveline, Ratchetaxis: Long-Range Directed Cell Migration by Local Cues, Trends Cell Biol. 25 (2015) 815–827. https://doi.org/10.1016/j.tcb.2015.10.009.

[Callens2020] S.J.P. Callens, R.J.C. Uyttendaele, L.E. Fratila-Apachitei, A.A. Zadpoor, Substrate curvature as a cue to guide spatiotemporal cell and tissue organization, Biomaterials. 232 (2020) 119739. https://doi.org/10.1016/j.biomaterials.2019.119739.

[Chandorkar2019] Y. Chandorkar, A. Castro Nava, S. Schweizerhof, M. Van Dongen, T. Haraszti, J. Köhler, H. Zhang, R. Windoffer, A. Mourran, M. Möller, L. De Laporte, Cellular responses to beating

hydrogels to investigate mechanotransduction, Nat. Commun. 10 (2019) 4027. https://doi.org/10.1038/s41467-019-11475-4.
[Chelberg1989] CHELBERG, M. K. et EC, Tsilibary. Hauser AR. McCarthy JB. Type 1V collagen-mediated melanoma cell adhesion and migration: involvement of multiple. distinct domains of the collagen molecule. Cancer Res, 1989, vol. 49, p. 4796-4802.
[Chevalier2018] N.R. Chevalier, The first digestive movements in the embryo are mediated by mechanosensitive smooth muscle calcium waves, Philos. Trans. R. Soc. B Biol. Sci. 373 (2018) 20170322. https://doi.org/10.1098/rstb.2017.0322.
[Davidson2020] P.M. Davidson, B. Cadot, Actin on and around the Nucleus, Trends Cell Biol. 31 (2021) 211–223. https://doi.org/10.1016/j.tcb.2020.11.009.
[Deguchi2006] S. Deguchi, T. Ohashi, M. Sato, Tensile properties of single stress fibers isolated from cultured vascular smooth muscle cells, J. Biomech. 39 (2006) 2603–2610. https://doi.org/10.1016/j.jbiomech.2005.08.026.
[Devreotes2003] P. Devreotes & C. Janetopoulos. Eukaryotic Chemotaxis: Distinctions between Directional Sensing and Polarization. Journal of Biological Chemistry, Volume 278, Issue 23, 20445 - 20448 https://doi.org/10.1074/jbc.R300010200
[Dokukina2010] I.V. Dokukina, M.E. Gracheva, A model of fibroblast motility on substrates with different rigidities, Biophys. J. 98 (2010) 2794–2803. https://doi.org/10.1016/j.bpj.2010.03.026.
[Dubois2006] F. Dubois, M. Jean, The non smooth contact dynamic method: recent LMGC90 software developments and application, in: P.W.P. Dr, U.N.P. Dr (Eds.), Anal. Simul. Contact Probl., Springer Berlin Heidelberg, 2006: pp. 375–378. https://doi.org/10.1007/3-540-31761-9_44.
[Gittes1993] F. Gittes, B. Mickey, J. Nettleton, J. Howard, Flexural rigidity of microtubules and actin filaments measured from thermal fluctuations in shape., J. Cell Biol. 120 (1993) 923–934. https://doi.org/10.1083/jcb.120.4.923.
[Han2012] S.J. Han, K.S. Bielawski, L.H. Ting, M.L. Rodriguez, N.J. Sniadecki, Decoupling Substrate Stiffness, Spread Area, and Micropost Density: A Close Spatial Relationship between Traction Forces and Focal Adhesions, Biophys. J. 103 (2012) 640–648. https://doi.org/10.1016/j.bpj.2012.07.023.
[Harmand2021] N. Harmand, A. Huang, S. Hénon, 3D Shape of Epithelial Cells on Curved Substrates, Phys. Rev. X. 11 (2021) 031028. https://doi.org/10.1103/PhysRevX.11.031028.
[Hersen2011] Hersen P et Ladoux B Nature 2011, Push it, pull it, Nature. 470 (2011) 340–341. https://doi.org/10.1038/470340a.
[Isenberg2009] B.C. Isenberg, P.A. DiMilla, M. Walker, S. Kim, J.Y. Wong. Vascular Smooth Muscle Cell Durotaxis Depends on Substrate Stiffness Gradient Strength. Biophysical Journal, Volume 97, Issue 5, 1313 – 1322 https://doi.org/10.1016/j.bpj.2009.06.021
[Jaffe1998] L.F. Jaffe, R. Créton, On the conservation of calcium wave speeds, Cell Calcium. 24 (1998) 1–8. https://doi.org/10.1016/S0143-4160(98)90083-5.
[Jaffe2008] L.F. Jaffe, Calcium waves, Philos. Trans. R. Soc. B Biol. Sci. 363 (2008) 1311–1317. https://doi.org/10.1098/rstb.2007.2249.
[Jean1999] M. Jean, The non-smooth contact dynamics method, Comput. Methods Appl. Mech. Eng. 177 (1999) 235–257. https://doi.org/10.1016/S0045-7825(98)00383-1.
[Jiang2005] X. Jiang, D.A. Bruzewicz, A.P. Wong, M. Piel, and G.M. Whitesides. Directing cell migration with asymmetric micropatterns. PNAS 2005, vol.102, no.4, p975–978. https://doi.org/10.1073/pnas.0408954102
[Kishi2014] K. Kishi, T.A. Onuma, H. Nishida, Long-distance cell migration during larval development in the appendicularian, Oikopleura dioica, Dev. Biol. 395 (2014) 299–306. https://doi.org/10.1016/j.ydbio.2014.09.006.

[le Digabel2011] J. le Digabel, N. Biais, J. Fresnais, J.-F. Berret, P. Hersen, B. Ladoux, Magnetic micropillars as a tool to govern substrate deformations, Lab. Chip. 11 (2011) 2630–2636. https://doi.org/10.1039/c1lc20263d.

[Lo2000] Lo, C.M., Wang H.B., Dembo, M., Wang, Y.I. Cell Movement Is Guided by the Rigidity of the Substrate. Biophysical Journal, Volume 79, Issue 1, 144 - 152 https://doi.org/10.1016/S0006-3495(00)76279-5

[Löber2014] J. Löber, F. Ziebert and I.S. Aranson. Modeling crawling cell movement on soft engineered substrates. Soft Matter, Issue 9, 2014

[Luxton2010] G.W.G. Luxton, E.R. Gomes, E.S. Folker, E. Vintinner, G.G. Gundersen, Linear Arrays of Nuclear Envelope Proteins Harness Retrograde Actin Flow for Nuclear Movement, Science. 329 (2010) 956–959. https://www.science.org/doi/10.1126/science.1189072.

[Malheiro2016] V. Malheiro, F. Lehner, V. Dinca, P. Hoffmann, K. Maniura-Weber, Convex and concave micro-structured silicone controls the shape, but not the polarization state of human macrophages, Biomater. Sci. 4 (2016) 1562–1573. https://doi.org/10.1039/C6BM00425C.

[Marzban2019] B. Marzban, J. Kang, N. Li, Y. Sun, H. Yuan, A contraction–reaction–diffusion model: Integrating biomechanics and biochemistry in cell migration, Extreme Mech. Lett. 32 (2019) 100566. https://doi.org/10.1016/j.eml.2019.100566.

[Mayor2016] R. Mayor, S. Etienne-Manneville, The front and rear of collective cell migration, Nat. Rev. Mol. Cell Biol. 17 (2016) 97–109. https://doi.org/10.1038/nrm.2015.14.

[Milan2016] J.-L. Milan, I. Manifacier, K.M. Beussman, S.J. Han, N.J. Sniadecki, I. About, P. Chabrand, In silico CDM model sheds light on force transmission in cell from focal adhesions to nucleus, J. Biomech. (2016). https://doi.org/10.1016/j.jbiomech.2016.05.031.

[Otrock2007] Z.K. Otrock, R.A.R. Mahfouz, J.A. Makarem, A.I. Shamseddine, Understanding the biology of angiogenesis: Review of the most important molecular mechanisms, Blood Cells. Mol. Dis. 39 (2007) 212–220. https://doi.org/10.1016/j.bcmd.2007.04.001.

[Patan2004] S. Patan, Vasculogenesis and Angiogenesis, in: M. Kirsch, P.McL. Black (Eds.), Angiogenesis Brain Tumors, Springer US, Boston, MA, 2004: pp. 3–32. https://doi.org/10.1007/978-1-4419-8871-3_1.

[Park2018] J.S., Park, D.H. Kim, A. Levchenko. Topotaxis: A New Mechanism of Directed Cell Migration in Topographic ECM Gradients. Biophysical Journal, Volume 114, Issue 6, 1257 – 1263 https://doi.org/10.1016/j.bpj.2017.11.3813

[Pieuchot2018] L. Pieuchot, J. Marteau, A. Guignandon, T. Dos Santos, I. Brigaud, P.-F. Chauvy, T. Cloatre, A. Ponche, T. Petithory, P. Rougerie, M. Vassaux, J.-L. Milan, N. Tusamda Wakhloo, A. Spangenberg, M. Bigerelle, K. Anselme, Curvotaxis directs cell migration through cell-scale curvature landscapes, Nat. Commun. 9 (2018) 3995. https://doi.org/10.1038/s41467-018-06494-6.

[Raghavan2010] S. Raghavan, R.A. Desai, Y. Kwon, M. Mrksich, C.S. Chen, Micropatterned Dynamically Adhesive Substrates for Cell Migration, Langmuir. 26 (2010) 17733–17738. https://doi.org/10.1021/la102955m.

[Reversat2020] Reversat, A., Gaertner, F., Merrin, J. et al. Cellular locomotion using environmental topography. Nature 582, 582–585 (2020). https://doi.org/10.1038/s41586-020-2283-z

[Ribeiro2016] A.J.S. Ribeiro, A.K. Denisin, R.E. Wilson, B.L. Pruitt, For whom the cells pull: Hydrogel and micropost devices for measuring traction forces, Methods. (2016). https://doi.org/10.1016/j.ymeth.2015.08.005.

[Rougerie2020] P. Rougerie, L. Pieuchot, R.S. dos Santos, J. Marteau, M. Bigerelle, P.-F. Chauvy, M. Farina, K. Anselme, Topographical curvature is sufficient to control epithelium elongation, Sci. Rep. 10 (2020) 14784. https://doi.org/10.1038/s41598-020-70907-0.

[Scarpa2016] E. Scarpa, R. Mayor, Collective cell migration in development, J. Cell Biol. 212 (2016) 143–155. https://doi.org/10.1083/jcb.201508047.

[Schamberger2023] Schamberger et al. Curvature in Biological Systems: Its quantification, Emergence and Implications Across the Scales, Advanced Materials 2023. https://doi.org/10.1002/adma.202206110

[SenGupta2021] S. SenGupta, C.A. Parent, J.E. Bear, The principles of directed cell migration, Nat. Rev. Mol. Cell Biol. 22 (2021) 529–547. https://doi.org/10.1038/s41580-021-00366-6.

[Shellard2020] A. Shellard, R. Mayor, All Roads Lead to Directional Cell Migration, Trends Cell Biol. 30 (2020) 852–868. https://doi.org/10.1016/j.tcb.2020.08.002.

[Shellard2018] A. Shellard, A. Szabó, X. Trepat, R. Mayor, Supracellular contraction at the rear of neural crest cell groups drives collective chemotaxis, Science. 362 (2018) 339–343. https://doi.org/10.1126/science.aau3301.

[Shellard2019] A. Shellard, R. Mayor, Supracellular migration – beyond collective cell migration, J. Cell Sci. 132 (2019). https://doi.org/10.1242/jcs.226142.

[Sokolow2012] A. Sokolow, Y. Toyama, D.P. Kiehart, G.S. Edwards, Cell Ingression and Apical Shape Oscillations during Dorsal Closure in Drosophila, Biophys. J. 102 (2012) 969–979. https://doi.org/10.1016/j.bpj.2012.01.027.

[Szabó2016] A. Szabó, M. Melchionda, G. Nastasi, M.L. Woods, S. Campo, R. Perris, R. Mayor, In vivo confinement promotes collective migration of neural crest cells, J. Cell Biol. 213 (2016) 543–555. https://doi.org/10.1083/jcb.201602083.

[Theveneau2012] E. Theveneau, R. Mayor, Neural crest migration: interplay between chemorepellents, chemoattractants, contact inhibition, epithelial–mesenchymal transition, and collective cell migration, WIREs Dev. Biol. 1 (2012) 435–445. https://doi.org/10.1002/wdev.28.

[Tomba2019] C. Tomba, T. Petithory, R. Pedron, A. Airoudj, I. Di Meglio, A. Roux, V. Luchnikov. In Laser-Assisted Strain Engineering of Thin Elastomer Films to Form Variable Wavy Substrates for Cell Culture. Small 15 21 (2019): e1900162 https://doi.org/10.1002/smll.201900162

[Tjhung2015] E. Tjhung, A. Tiribocchi, D. Marenduzzo, M.E. Cates, A minimal physical model captures the shapes of crawling cells, Nat. Commun. 6 (2015) 5420. https://doi.org/10.1038/ncomms6420.

[Vassaux2019] M. Vassaux, L. Pieuchot, K. Anselme, M. Bigerelle, J.-L. Milan, A Biophysical Model for Curvature-Guided Cell Migration, Biophys. J. 117 (2019) 1136–1144. https://doi.org/10.1016/j.bpj.2019.07.022.

[Vassaux2018] Maxime Vassaux. (2018). mvassaux/adhSC: Initial release of the adhesion cell model (v1.0.0). Zenodo. https://doi.org/10.5281/zenodo.1187087

[Wakhloo2020] N. T. Wakhloo, S. Anders, F. Badique, M. Eichhorn, I. Brigaud, T. Petithory, M. Vassaux, J. L. Milan, J.N. Freund, J. Rühe, P.M. Davidson, L. Pieuchot, K. Anselme. Actomyosin, vimentin and LINC complex pull on osteosarcoma nuclei to deform on micropillar topography. Biomaterials 234 (2020) 119746.

[Winkler2019] B. Winkler, I.S. Aranson, F. Ziebert, Confinement and substrate topography control cell migration in a 3D computational model, Commun. Phys. 2 (2019) 1–11. https://doi.org/10.1038/s42005-019-0185-x.

[Werner2019] M. Werner, A. Petersen, N.A. Kurniawan, C.V.C. Bouten, Cell-Perceived Substrate Curvature Dynamically Coordinates the Direction, Speed, and Persistence of Stromal Cell Migration, Adv. Biosyst. 3 (2019) 1900080. https://doi.org/10.1002/adbi.201900080.

[Zhang2017] J. Zhang, Y.l. Wang. Centrosome defines the rear of cells during mesenchymal migration. Molecular Biology of the Cell 2017 28:23, 3240-3251